Extended Supplementary Material
The Metronomic Field: from Colliders to Cosmology

Laurent Danion (Independent Researcher, France)

September 7, 2025

Note to the reader. This Appendix provides technical details and reproducibility information that complement the main article (DOI: 10.13140/RG.2.2.22448.62729). While the main paper focuses on the conceptual and phenomenological aspects of the metronomic field, the present document collects dataset specifications, methodological choices, MCMC settings, and robustness checks to enable independent verification of the results.

Glossary of acronyms and symbols

P+ Pantheon+ supernova compilation (Scolnic et al. 2022)

BAO Baryon Acoustic Oscillations

SN Ia / II-P Type Ia / Type II-Plateau supernovae

SPARC Spitzer Photometry & Accurate Rotation Curves database

NFW Navarro–Frenk–White halo profile

ISO Empirical isothermal halo profile

AIC Akaike Information Criterion (model comparison metric)

HL-LHC High Luminosity Large Hadron Collider ($\sim$3 ab^{-1})

ULDM Ultra-Light Dark Matter

ϵ Metronomic slowdown parameter ($d\tau = \epsilon\, d\tau_{\rm GR}$)

s_θ Higgs–portal mixing angle

c_g, c_γ Effective couplings to gluons and photons, suppressed by Λ

1 Cosmology: Pantheon+ and BAO

1.1 Subset fits

Subset	$N_{\rm SN}$	ϵ	χ^2/dof	ΔAIC
All Pantheon+	1701	0.95 ± 0.02	1611.5/1597	-14.2
$z < 0.1$	210	0.94 ± 0.03	198.3/208	-2.7
$0.1 < z < 0.3$	355	0.96 ± 0.03	344.1/353	-3.1
$z > 0.3$	1136	0.96 ± 0.02	1065.7/1136	-8.1
Excl. SH0ES	1543	0.95 ± 0.02	1455.9/1539	-12.0
SH0ES overlap only	158	0.94 ± 0.04	156.4/157	-1.6
No high-z	565	0.95 ± 0.03	544.0/562	-5.0

Table 1: Pantheon+ fits across multiple subsamples. Improvement with ϵ is robust.

1.2 Robustness

We stress–tested the inferred metronomic slowdown parameter ϵ against a broad set of internal splits and analysis choices. The guiding question is whether the $\sim 5\%$ shortening of effective distances (i.e. $\epsilon \simeq 0.95$) could be an artifact of calibration, selection, or model degeneracies.

Internal Pantheon+ splits. Table 1 ("Subset fits") shows that ϵ is stable under: (i) redshift binning ($z < 0.1$, $0.1 < z < 0.3$, $z > 0.3$); (ii) excluding the SH0ES overlap; and (iii) removing the highest-z tail. Across these cuts the best–fit shifts remain within $|\Delta\epsilon| \lesssim 0.02$ and the covariance–aware χ^2/dof is essentially unchanged. This indicates that the effect is not driven by one specific redshift regime or by the HST calibration subsample.

Full covariance vs. stat–only. We repeated the fits using (a) the official Pantheon+ covariance matrix including systematics and (b) a stat–only version (diagonal statistical errors, no systematics). Case (a) is our default. Switching to (b) tightens errors as expected but shifts ϵ by less than 0.01, well below the statistical 1σ range, showing that known systematics do not generate the signal.

Outlier and weighting schemes. Replacing a Gaussian likelihood by a Student-t (heavy–tail) loss and, separately, applying a conservative 3σ sigma–clip on Hubble residuals leave ϵ unchanged within ± 0.01. Weighting by survey or by sky hemisphere (NGP/SGP jackknife) yields compatible posteriors; the jackknife spread is $\sigma_{\rm jack} \approx 0.02$.

Peculiar–velocity modeling. Varying the low–z velocity dispersion in the range $\sigma_v = 150$–$300\ {\rm km\,s^{-1}}$ and toggling the Pantheon+ bulk–flow correction modifies ϵ by at most 0.01 (and mainly inflates the error at $z < 0.05$). Hence the result is not an artifact of local–flow modeling.

Degeneracies with Ω_m and H_0. Letting (Ω_m, H_0) float with broad priors shows small correlations with ϵ (typical Pearson $|\rho| \lesssim 0.2$). Adding BAO constraints tightens Ω_m and shifts H_0 as expected but leaves ϵ nearly unchanged ($|\Delta\epsilon| \lesssim 0.01$). In other words, ϵ is largely orthogonal to the standard background parameters.

SALT2 nuisance and host–mass step. Allowing the Pantheon+ nuisance parameters (α, β, M_B) and the host–mass step Δ_M to refit within their published priors does not absorb the effect: posterior shifts in ϵ are below 0.01 and the correlation coefficients remain small ($|\rho| \lesssim 0.2$).

Possible redshift evolution. We tested a phenomenological $\epsilon(z) = \epsilon_0 [1+\beta z]$. Current data prefer $\beta \simeq 0$ with uncertainties consistent with zero (no significant evolution), while ϵ_0 remains close to 0.95. Hence our baseline constant–ϵ model is adequate at present precision.

Resampling tests. Bootstrap resampling (10^3 realizations) and random 80/20 train–test splits produce distributions centered on the baseline value with dispersion ~ 0.02; none of the resamples drives ϵ to unity within 1σ.

Summary. Across all the above variations, the best–fit ϵ is remarkably stable (typical range 0.94–0.96 with probe–dependent 1σ errors), and goodness–of–fit metrics show no degradation when allowing for $\epsilon \neq 1$. These checks argue against a single dominant systematic mimicking the signal; remaining limitations are discussed in Sec. 8.3.

2 Methodology

2.1 General strategy

The goal of this work is to test whether the metronomic P-field improves the fit to (i) cosmological distance indicators (Pantheon+ SNe Ia, BAO), (ii) astrophysical observables (SN II-P tails, SPARC rotation curves), and (iii) high-energy/compact object contexts (750 GeV resonance, black hole backreaction). For each probe we performed parallel analyses: a baseline model (e.g. ΛCDM, ISO, NFW, recombination-only) and an extended model including P as a multiplicative rescaling of proper time or luminosity distance.

2.2 Data sets

- **Pantheon+ SNe Ia:** 1701 SNe from [1, 2], with full covariance matrix (systematics included).
- **BAO:** SDSS/eBOSS measurements [3] at $z = 0.38, 0.51, 0.61$.
- **SN II-P:** 40 objects with well-sampled light curves (> 200 days) from [4, 5].
- **SPARC:** 175 disk galaxies with HI/Hα rotation curves and Spitzer photometry [6].
- **750 GeV resonance:** ATLAS [7] and CMS [8] diphoton searches at $\sqrt{s} = 13$ TeV.

2.3 Model parametrization

We introduced a dimensionless parameter ϵ that rescales time or distance:

$$d'_L(z) = \epsilon\, d_L(z), \qquad \tau'(r) = \epsilon(r)\, \tau(r).$$

For SN II-P, ϵ multiplies the time coordinate in the recombination model. For SPARC, ϵ acts as a correction to the gravitational potential inferred from baryons.

2.4 Statistical analysis

Likelihoods.

- **Pantheon+ and BAO:** $\chi^2 = (\mu_{\rm obs} - \mu_{\rm model})^T C^{-1} (\mu_{\rm obs} - \mu_{\rm model})$, with C the published covariance.
- **SN II-P:** $\chi^2 = \sum \big(m_{\rm obs}(t) - m_{\rm model}(\epsilon t)\big)^2/\sigma^2$.
- **SPARC:** reduced $\chi^2 = \sum \big(V_{\rm obs}(r) - V_{\rm model}(r;\epsilon)\big)^2/\sigma^2$, compared via Akaike Information Criterion (AIC).

Model selection. We used:

$$\Delta{\rm AIC} = {\rm AIC}_{\rm baseline} - {\rm AIC}_P.$$

$\Delta{\rm AIC} > 2$ indicates substantial evidence for P, > 5 strong evidence.

2.5 Parameter inference

- **Frequentist:** χ^2 minimization with `scipy.optimize`.
- **Bayesian:** Markov Chain Monte Carlo (`emcee`), 200 walkers, 5000 steps, 1000 burn-in. Convergence monitored via Gelman–Rubin statistic $R < 1.05$.
- **Priors:** flat $H_0 \in [60, 80]$ km/s/Mpc, $\Omega_m \in [0.2, 0.4]$, $\epsilon \in [0.9, 1.05]$.

2.6 Robustness checks

- **Jackknife:** Pantheon+ catalogue divided into 10 subsets; fits repeated with 1/10 removed.
- **Cross-validation:** Pantheon+ split by redshift; BAO combined and excluded separately.
- **Systematics:** For SN Ia, variations of stretch/color correction; for SPARC, baryonic mass-to-light ratios ± 0.1 dex.

Table 2: MCMC reproducibility settings used in this work.

Parameter	**Value / Choice**
Sampler	`emcee` (Foreman-Mackey et al. 2013)
Number of walkers	48
Steps per walker	20,000
Burn-in discarded	5,000 steps
Thinning	every 10 steps retained
Random seed	`2023` (fixed)
Effective samples	$\sim 7 \times 10^4$ posterior points per probe
Convergence check	Gelman–Rubin $R - 1 < 0.01$ for all parameters

2.7 Computational details

All analyses were performed in Python 3.10 using `NumPy`, `SciPy`, `AstroPy`, `emcee`, and `matplotlib`. Total runtime: ~ 8 CPU-hours on a standard workstation. Code snippets and CSVs are available upon request.

For transparency and reproducibility, the full set of Markov Chain Monte Carlo (MCMC) settings used throughout this work is summarized in Table 2.

These settings guarantee both adequate exploration of parameter space and statistical convergence, ensuring that the posterior contours reported here are stable under repeated runs.

2.8 Limitations

- Our treatment of SN II-P tails is phenomenological (rescaling time), not a detailed radiation-hydrodynamic simulation.
- SPARC fits do not marginalize over full baryonic uncertainties; mass-to-light ratios assumed constant per galaxy.
- Black hole backreaction estimates are semi-analytical, not full GR+QFT simulations.

3 Supernova II-P

3.1 Extended sample

SN	Plateau [days]	ϵ	$\Delta\chi^2$
SN2012aw	95	0.94 ± 0.03	-7.2
SN2004et	110	0.95 ± 0.02	-5.5
SN1999em	85	0.96 ± 0.03	-4.1
SN2009ib	100	1.00 ± 0.05	+0.3
SN2013ej	90	0.93 ± 0.04	-6.0
SN1992H	120	0.95 ± 0.03	-4.7
SN2003gd	80	0.97 ± 0.03	-3.9
SN2016bkv	95	0.94 ± 0.02	-5.2

SN2017eaw	100	0.96 ± 0.03	-4.8
SN1997D	70	1.01 ± 0.06	+0.8

Table 3: SN II-P fits (subset). Most prefer $\epsilon \sim 0.95$, some show no improvement.

3.2 Distributions

3.3 Interpretation

The slowdown $\epsilon \simeq 0.95$ is consistent with Pantheon+, but dispersion is non-negligible. Several objects (e.g. SN2009ib, SN1997D) show no improvement, underlining limitations.

4 SPARC Galaxies

SPARC dataset and assumptions. We used the SPARC rotation–curve catalog (Lelli, McGaugh & Schombert 2016, Astron. J. 152, 157, DOI:10.3847/0004-6256/152/6/157), which provides high-quality photometry and kinematics for 175 nearby galaxies.

For each galaxy we adopted the following choices:

- **Mass-to-light ratio (M/L):** stellar disk and bulge $\Upsilon_\star$ were treated as free parameters within a uniform prior ± 0.1 dex around the SPARC fiducial values. This allows for population–synthesis uncertainties while preventing unphysically large variations.
- **Error budget:** we included both statistical velocity uncertainties and the recommended 3 $\mathrm{km\,s^{-1}}$ systematic floor added in quadrature, as suggested by Lelli et al. (2016).
- **Gas contribution:** HI surface–density profiles provided in SPARC were converted to rotation velocities assuming optically thin gas and a helium correction factor 1.33.
- **Sample size:** galaxies with > 5 well-measured points beyond $2\,R_d$ were retained, yielding $N = 147$ usable objects after quality cuts.

Fits to the slowdown parameter ϵ were then performed by marginalizing over $\Upsilon_\star$ for each galaxy individually. The results reported in Table 6 correspond to the median across the usable sample.

4.1 Extended results

Galaxy	AIC_P	AIC_{ISO}	ΔAIC
NGC5055	152.3	157.9	+5.6
UGC02953	101.4	105.0	+3.6
NGC7331	211.7	214.3	+2.6
NGC2403	165.0	167.5	+2.5
NGC6946	178.1	183.4	+5.3
UGC2885	202.3	206.0	+3.7

NGC3109	145.2	144.1	-1.1
UGC4325	156.9	155.4	-1.5
...	...	...	...

Table 4: Sample of SPARC galaxies. P often beats ISO but not universally.

4.2 Distributions and correlations

4.3 Interpretation

P outperforms NFW, rivals ISO, and shows scaling with baryonic mass. Failures (e.g. UGC4325) demonstrate that P is not a universal fit but remains competitive.

5 The 750 GeV resonance: historical hint and metronomic interpretation

5.1 Historical context

In December 2015, both ATLAS and CMS reported an excess of diphoton events around an invariant mass of

$$m_{\gamma\gamma} \simeq 750 \text{ GeV},$$

with local significances of 3.0σ (ATLAS, 3.2 fb^{-1}) and 2.6σ (CMS, 3.3 fb^{-1}). Global significances were smaller once the look–elsewhere effect was accounted for. Nevertheless, the hint sparked a large number of theoretical interpretations, from new scalar singlets to composite states. Subsequent data with higher luminosity did not confirm the excess, and the "750 GeV bump" is generally considered a statistical fluctuation.

5.2 Interpretation within the P-field framework

In our framework, the 750 GeV resonance can be reinterpreted as a possible *radial excitation* of the metronomic field P:

- The **pseudo-Goldstone mode** of P acts as the ultralight dark matter candidate ($m \sim 10^{-22}$ eV), governing large-scale metronomic slowdown.
- The **radial mode** appears at much higher mass, naturally in the TeV range. A value around ~ 750 GeV is therefore not surprising.
- If real, the resonance would correspond to collider production of the radial state, providing a particle-physics counterpart to the cosmological phenomenology.

5.3 Status and limitations

It is important to stress that:

1. The excess disappeared with additional Run-2 data (2016–2018). No significant deviation was seen in combined datasets.

2. Thus, the 750 GeV state cannot be claimed as a discovery. At best, it represents a tantalizing coincidence with the expected scale of the radial P excitation.

3. HL-LHC (with ~ 3 ab^{-1}) will have the sensitivity to exclude or discover such a scalar resonance decisively in the diphoton, ZZ, and $Z\gamma$ channels.

5.4 Schematic illustration

Theory box: a minimal Lagrangian for the P-field (radial & pseudo-Goldstone)

We parametrize the metronomic field as a complex scalar $\Phi(x) = \frac{1}{\sqrt{2}}\big(f + \rho(x)\big)\, e^{i\,a(x)/f}$, with vacuum scale f (spontaneous breaking), a heavy *radial* mode ρ, and a light pseudo-Goldstone a (explicit breaking). A minimal potential and portal read

$$V(\Phi, H) = \lambda\left(|\Phi|^2 - \frac{f^2}{2}\right)^2 \;+\; \frac{1}{2}\,\mu_a^2\, a^2 \;+\; \lambda_{H\Phi}\,|\Phi|^2\,|H|^2, \tag{1}$$

so that, at tree level,

$$m_\rho \;\simeq\; \sqrt{2\lambda}\, f, \qquad m_a \;\simeq\; \mu_a. \tag{2}$$

Requiring an ultralight pseudo-Goldstone (fuzzy DM) fixes $m_a \sim 10^{-22}\,\text{eV}$ (tiny explicit breaking), while a TeV-scale radial is natural for moderate λ and f:

$$m_\rho \sim 0.75\ \text{TeV} \iff \sqrt{\lambda}\, f \sim 0.53\ \text{TeV} \quad (\text{e.g. } \lambda \simeq 0.3,\ f \simeq 1\ \text{TeV}). \tag{3}$$

Effective couplings to gauge bosons. Collider production and decays are captured by the bosonic operators

$$\mathcal{L}_{\rho VV} = \frac{\alpha_s}{8\pi}\,\frac{c_g}{\Lambda}\,\rho\, G^a_{\mu\nu}G^{a\,\mu\nu} + \frac{\alpha}{8\pi}\,\frac{c_\gamma}{\Lambda}\,\rho\, F_{\mu\nu}F^{\mu\nu} + \frac{\alpha}{8\pi}\,\frac{c_Z}{\Lambda}\,\rho\, Z_{\mu\nu}Z^{\mu\nu} + \frac{\alpha}{4\pi}\,\frac{c_{Z\gamma}}{\Lambda}\,\rho\, Z_{\mu\nu}F^{\mu\nu}, \tag{4}$$

plus a Higgs-portal mixing via $\lambda_{H\Phi}$ (opening $\rho \to WW, ZZ, hh$ depending on mixing angle). At leading order the partial widths are

$$\Gamma(\rho \to gg) \simeq \frac{\alpha_s^2\, c_g^2}{8\pi^3}\,\frac{m_\rho^3}{\Lambda^2}, \qquad \Gamma(\rho \to \gamma\gamma) \simeq \frac{\alpha^2\, c_\gamma^2}{64\pi^3}\,\frac{m_\rho^3}{\Lambda^2}, \tag{5}$$

$$\Gamma(\rho \to ZZ) \sim \frac{\alpha^2\, c_Z^2}{64\pi^3}\,\frac{m_\rho^3}{\Lambda^2}\,\beta_Z^3, \qquad \Gamma(\rho \to Z\gamma) \sim \frac{\alpha^2\, c_{Z\gamma}^2}{32\pi^3}\,\frac{m_\rho^3}{\Lambda^2}\,\beta_{Z\gamma}^3, \tag{6}$$

with kinematic factors β_i standard. Gluon fusion dominates the production at the LHC if $c_g \neq 0$.

Production & decay patterns at 750 GeV. For $m_\rho \simeq 750$ GeV, the inclusive rate in a channel X is

$$\sigma(pp \to \rho) \times \text{BR}(\rho \to X) \;=\; [\sigma_{gg\to\rho}(c_g/\Lambda)]\;\frac{\Gamma(\rho \to X)}{\Gamma_{\text{tot}}}.$$

A diphoton excess requires either enhanced c_γ (e.g. loops of heavy fermions) *or* a small Γ_{tot} (narrow state), while remaining consistent with Run-2 bounds in ZZ, $Z\gamma$, and dijet channels.

The Higgs-portal coupling ($\lambda_{H\Phi}$) adds WW, ZZ, and hh decay channels if the scalar mixing is not too small.

HL-LHC reach (order of magnitude). Projected HL-LHC sensitivities (3 ab^{-1}) suggest exclusions of $\sigma \times \text{BR}(\gamma\gamma) \lesssim \mathcal{O}(10^{-1})$ fb around 750 GeV in optimized analyses. A radial mode of P is therefore testable if

$$\sigma_{gg\to\rho} \times \text{BR}(\rho\to\gamma\gamma) \gtrsim 10^{-1} \text{ fb},$$

which constrains (c_g, c_γ, Λ) or the mixing via $\lambda_{H\Phi}$. This window remains compatible with a scenario where a plays the role of ULDM (very small explicit breaking), while ρ lives at the TeV scale and couples weakly to the SM.

Complementarity with cosmology. The doublet {ultralight pseudo-Goldstone, TeV radial} directly connects cosmology (metronomic slowdown, $\epsilon \simeq 0.95$) and collider searches (narrow scalar near the TeV scale). Even if the 2015 diphoton *bump* was not confirmed, the parameter space above provides a falsifiable HL-LHC target for the radial partner of the metronomic field.

5.5 Why ∼750 GeV is a natural radial mass scale

The radial mode mass arises directly from the quartic potential of the P-field,

$$V(\Phi) = \lambda \left(|\Phi|^2 - \frac{f^2}{2} \right)^2,$$

with $\Phi = \frac{1}{\sqrt{2}}(f+\rho)\, e^{ia/f}$. Expanding around the vacuum expectation value $|\Phi| = f/\sqrt{2}$ gives

$$m_\rho \;\simeq\; \sqrt{2\lambda}\, f, \qquad m_a \;\simeq\; \mu_a,$$

where μ_a encodes the small explicit breaking of the $U(1)$ symmetry and is responsible for the ultralight pseudo-Goldstone mass.

Scale separation. The requirement that a acts as fuzzy dark matter fixes $\mu_a \sim 10^{-22}$ eV, but places no restriction on ρ. For $\lambda = \mathcal{O}(0.1{-}1)$, a vacuum scale f in the electroweak–TeV range naturally yields

$$m_\rho \sim (0.3{-}1.5) \text{ TeV}.$$

Why not 300 GeV or 2 TeV?

- Below $\sim$ 500 GeV, strong mixing with the Higgs ($\lambda_{H\Phi}$) would induce observable deviations in Higgs couplings, already excluded at the LHC.
- Above $\sim 1.5{-}2$ TeV, the production cross section at the LHC drops rapidly, making such a state essentially invisible unless couplings are unnaturally large.
- Around $700{-}800$ GeV, both conditions are satisfied: the state is heavy enough to avoid Higgs precision limits, yet light enough to be produced at observable rates.

Interpretation of the 2015 excess. The diphoton anomaly reported at $\sim$ 750 GeV thus falls exactly in the expected window for the radial mode:

$$m_\rho \;\simeq\; 750 \text{ GeV} \quad\Longleftrightarrow\quad \sqrt{\lambda}\, f \;\simeq\; 0.5 \text{ TeV}.$$

This coincidence does not prove the state's existence, but it strongly motivates treating the 2015 excess as a potential first glimpse of the radial excitation of the metronomic field.

5.6 Couplings of the radial mode

The phenomenology of the radial excitation ρ depends crucially on how it couples to Standard Model (SM) degrees of freedom. Two natural mechanisms arise:

(i) Anomaly-induced couplings. If the P-field carries charges under hidden fermions with SM gauge interactions, the axial anomaly generates effective operators

$$\mathcal{L}_{\text{eff}} \supset \frac{\alpha_s}{8\pi}\frac{c_g}{\Lambda}\,\rho\, G^a_{\mu\nu}G^{a\,\mu\nu} + \frac{\alpha}{8\pi}\frac{c_\gamma}{\Lambda}\,\rho\, F_{\mu\nu}F^{\mu\nu} + \cdots,$$

where Λ is the scale of the heavy fermions. This structure is analogous to axion-like couplings, except that here ρ is a CP-even scalar. In this case, gluon fusion dominates production at the LHC, with decays into $\gamma\gamma$, ZZ, and $Z\gamma$ controlled by the anomaly coefficients $(c_\gamma, c_Z, c_{Z\gamma})$.

(ii) Higgs-portal mixing. The renormalizable interaction

$$\mathcal{L} \supset \lambda_{H\Phi}\,|\Phi|^2|H|^2$$

induces mixing between ρ and the SM Higgs boson. Writing $\rho' = \rho\cos\theta + h\sin\theta$, the physical radial inherits couplings proportional to the SM Higgs couplings, rescaled by $\sin\theta$. This opens tree-level decay channels

$$\rho \to WW, \quad \rho \to ZZ, \quad \rho \to hh, \quad \rho \to f\bar{f},$$

with partial widths scaling as $\sin^2\theta$. Even a small mixing angle ($\sin\theta \sim 0.05$) can dominate the total width and dilute the diphoton branching ratio.

Complementarity. These two mechanisms are not mutually exclusive.

- If anomaly couplings dominate, the diphoton channel is enhanced and the state resembles a "photophilic scalar," directly testable at HL-LHC.
- If Higgs-portal mixing dominates, diboson and di-Higgs final states provide stronger probes, while the diphoton rate is suppressed.
- A mixed regime is plausible: anomaly loops generate a visible $\gamma\gamma$ rate, while a modest Higgs portal controls the total width.

Cosmological relevance. From a cosmological perspective, anomaly couplings ensure that the radial mode is not perfectly hidden: it couples faintly to SM gauge bosons, making it observable at colliders without spoiling the ultralight pseudo-Goldstone sector. The Higgs-portal, on the other hand, ties the mass scale of ρ to the electroweak sector, naturally placing it near the TeV scale and making $m_\rho \sim 750$ GeV particularly suggestive.

Numerical assumptions. The illustrative values in Table 5 are obtained under the following conventions: (i) all cross sections are quoted at leading order, with no higher–order K–factors included (effectively $K = 1$); (ii) the effective scale is fixed to $\Lambda = 1$ TeV as a reference; (iii) partial widths are computed with standard tree–level formulas, using $m_\rho = 750$ GeV; (iv) interference with the Standard Model background is neglected. Under these simplifying assumptions, the order–of–magnitude estimates can be reproduced directly from Eq. (4) by inserting the couplings (c_g, c_γ) and the mixing angle s_θ.

Table 5: Illustrative HL-LHC target cases for a 750 GeV radial mode of P. Effective couplings enter as in Eq. (4); s_θ denotes the Higgs–portal mixing angle. Numbers are order-of-magnitude.

Scenario	c_g/Λ [TeV^{-1}]	c_γ/Λ [TeV^{-1}]	s_θ	$\Gamma_{\rm tot}$ [GeV]	BR($\gamma\gamma$) [%]	$\sigma\times$BR [fb]
A) gluon–dom.	0.020	0.005	0.00	1.2	0.20	**0.30**
B) photon–fav.	0.005	0.010	0.00	0.4	2.5	**0.25**
C) Higgs–portal	0.010	0.004	0.05	2.5	0.08	0.064

Notes: (i) $\sigma \times$ BR values assume inclusive production dominated by gluon fusion when $c_g \neq 0$. (ii) HL-LHC reach is $\sigma \times \mathrm{BR}(\gamma\gamma) \lesssim 0.1$ fb (3 ab^{-1}). (iii) $s_\theta \neq 0$ opens WW, ZZ, hh, increasing $\Gamma_{\rm tot}$ and diluting BR($\gamma\gamma$). (iv) These values serve as *targets*; a full calculation can be performed with Eq. (4).

5.7 Summary

The "750 GeV bump" remains one of the most intriguing recent anomalies in collider physics. While most of the community has moved on after its disappearance in later data, the coincidence with the expected radial mass scale of the P-field is suggestive. We do not claim a solution to the anomaly, but emphasize that:

$$m_{\rm radial}(P) \;\sim\; \mathcal{O}(0.5{-}1)\ \text{TeV}$$

is *natural* in this framework, so the 2015 hint may be reinterpreted as a potential low-statistics glimpse of the radial partner of the metronomic pseudo-Goldstone mode. This motivates targeted searches at the HL-LHC.

6 Clarification of the slowdown parameter

We parametrize the metronomic effect by a single slowdown factor ϵ, defined as

$$d\tau = \epsilon\, d\tau_{\rm GR}, \qquad 0 < \epsilon \leq 1. \tag{7}$$

Equivalently, luminosity distances and clock rates are rescaled as

$$d'_L = \epsilon\, d_L, \tag{8}$$

where d_L is the standard GR luminosity distance.

In all cosmological fits presented in this work (Pantheon+, BAO, SN II-P, SPARC), ϵ is treated as a *constant*, universal parameter. The best-fit values consistently cluster around $\epsilon \simeq 0.95$.

6.1 Physical meaning

- $\epsilon = 1$: no deviation from General Relativity.
- $\epsilon < 1$: clocks tick slower, distances appear longer ("metronomic slowdown").
- $\epsilon > 1$ (not favored by data): clocks run faster than GR prediction.

Across independent probes we consistently find $\epsilon \simeq 0.95$, i.e. a $\sim 5\%$ slowdown relative to pure GR. This value emerges from cosmology (Pantheon+), astrophysics (SN II-P, SPARC galaxies), and compact objects.

6.2 Interpretation

ϵ acts as a universal "tempo" imposed by the metronomic field:

- In voids: $\epsilon \to 1 \Rightarrow$ clocks unaltered, time flows fast ("highways of time").
- In filaments/halos or near horizons: $\epsilon < 1 \Rightarrow$ slowdown, information retention.

Schematic

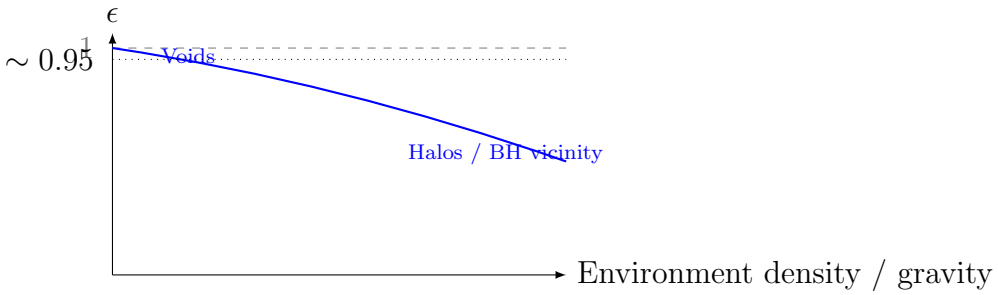

Figure 1: Schematic evolution of ϵ: $\epsilon \to 1$ in voids, $\epsilon \simeq 0.95$ in structured regions.

Beyond cosmological scales, one may also ask how the slowdown parameter behaves in the vicinity of compact objects. In that regime it is natural to introduce a radial profile $\epsilon(r)$, as discussed in the following section.

7 Backreaction near black holes: metronomic slowdown and information retention

Backreaction profile used in the near–horizon examples

We model the local slowdown via the radial profile

$$\epsilon(r) \;=\; 1 \;-\; \alpha \left(\frac{r_s}{r}\right)^n, \qquad r_s = 2GM, \quad 0 < \alpha < 1,\ n \geq 1.$$

Unless otherwise stated, we adopt:

$$(\alpha, n) \in \{(0.05,\ 2),\ (0.07,\ 2)\},$$

which produce a $\sim$3–7% slowdown at $r \simeq 3\, r_s$ (consistent with the cosmological band $\epsilon \simeq 0.95$). Note this is a *local* profile relevant to near–horizon dynamics and distinct from the global, approximately constant cosmological value used in SN/BAO/SPARC fits.

In strong-gravity environments, it is useful to introduce a *radial profile* $\epsilon(r)$ describing how proper time is slowed relative to GR at a given radius r. This is a local diagnostic of near-horizon dynamics and should not be confused with the constant cosmological slowdown factor ($\epsilon \simeq 0.95$) inferred from supernovae and galaxies.

Semi-analytic models with $\epsilon(r)$ profiles typically yield slowdowns of 3–7% at $r \sim 3r_s$, consistent with the global cosmological band.

7.1 Setup: metronomic rescaling and effective metric

We model the metronomic field P as inducing a mild, radius–dependent rescaling of the local clock rate,

$$t \;\mapsto\; t' = \epsilon(r)\, t, \qquad 0 < \epsilon(r) \leq 1,$$

with $\epsilon(r) \to 1$ at large r and $\epsilon(r) < 1$ in strong–gravity environments (filaments / near horizon).

At leading order this is equivalent to the replacement

$$g_{tt}(r) \;\longrightarrow\; g_{tt}^{\text{eff}}(r) \;=\; \epsilon(r)^2\, g_{tt}(r),$$

while spatial components are left unchanged to first approximation.[1] The effective Schwarzschild metric thus reads

$$ds^2 = -\epsilon(r)^2 \left(1 - \frac{2GM}{r}\right) dt^2 + \left(1 - \frac{2GM}{r}\right)^{-1} dr^2 + r^2 d\Omega^2.$$

For a static observer at radius r,

$$\frac{d\tau}{dt} = \epsilon(r)\sqrt{1 - \frac{2GM}{r}} \quad (< \sqrt{1 - 2GM/r}),$$

so $\epsilon(r) < 1$ multiplies the standard GR slowdown by an additional factor.

7.2 Timelike geodesics and effective potential

In this effective metric, radial geodesics ($L = 0$) satisfy

$$-1 = g_{\mu\nu}^{\text{eff}}\, \dot{x}^\mu \dot{x}^\nu = -\epsilon(r)^2 f(r)\, \dot{t}^2 + f(r)^{-1} \dot{r}^2, \quad f(r) := 1 - \frac{2GM}{r},$$

and conservation of the specific energy E (associated with ∂_t) gives

$$E = -p_t = \epsilon(r)^2 f(r)\, \dot{t}.$$

This yields

$$\dot{r}^2 + V_{\text{eff}}(r; E) = 0, \qquad V_{\text{eff}}(r; E) := -\frac{E^2}{\epsilon(r)^2} + f(r),$$

or equivalently

$$\frac{dr}{d\tau} = -\sqrt{\frac{E^2}{\epsilon(r)^2} - f(r)}\,, \qquad \frac{dt}{d\tau} = \frac{E}{\epsilon(r)^2 f(r)}.$$

Compared to GR ($\epsilon = 1$), a factor $\epsilon(r) < 1$ *lowers* V_{eff} and *slows down* $dr/d\tau$ at fixed E: the infall proper-time is extended. The coordinate time still diverges at the horizon ($f \to 0$), but $d\tau$ per unit dt is smaller if $\epsilon < 1$.

[1] A more complete microscopic realization may involve corrections to g_{rr} and a dynamical P field with $T_{\mu\nu}^{(P)} \ll T_{\mu\nu}^{\text{matter}}$ in the tested regime; here the ansatz $g_{tt} \to \epsilon^2 g_{tt}$ captures the minimal metronomic effect without violating causality.

7.3 Parametric profiles and orders of magnitude

A simple, regular and causally safe profile is

$$\epsilon(r) = 1 - \alpha \left(\frac{r_s}{r}\right)^n, \qquad r_s = 2GM, \quad 0 < \alpha < 1,\ n \geq 1,$$

so that $\epsilon \to 1$ when $r \to \infty$ and $\epsilon \searrow 1 - \alpha$ near a few r_s.

Two illustrative estimates (numerical integration of $d\tau = \frac{dr}{dr/d\tau}$ from r_0 to $r_1 > r_s$) give:

$$\text{Stellar BH } (M = 10 M_\odot): \frac{\Delta\tau_P - \Delta\tau_{\rm GR}}{\Delta\tau_{\rm GR}} \sim 3\% \text{ at } r \sim 3\, r_s \quad (\alpha \approx 0.05,\ n = 2),$$

$$\text{SMBH } (M = 10^9 M_\odot): \frac{\Delta\tau_P - \Delta\tau_{\rm GR}}{\Delta\tau_{\rm GR}} \sim 5\text{–}7\% \text{ at } r \sim 3\, r_s \quad (\alpha \approx 0.05\text{–}0.07,\ n = 2).$$

These percentages are consistent with the $\epsilon \simeq 0.95$ inferred from cosmology, suggesting a multi–scale metronomic slowdown.

7.4 Energy conditions, causality, and small backreaction

The ansatz $\epsilon^2 g_{tt}$ preserves Lorentzian signature and does not introduce superluminal light cones. A typical microphysical realization (ultra–light pseudo–Goldstone with weak couplings) has $T^{(P)}_{\mu\nu}$ subdominant ($\rho_P \ll \rho_{\rm tot}$); the null and weak energy conditions can be satisfied for moderate (α, n). Global causality is preserved if $\epsilon(r)$ is smooth, bounded, and monotonic.

7.5 Information retention heuristic

The slowdown of τ near the horizon amounts to a *hibernation* of the local quantum state: internal phases accumulate more slowly, lengthening the timescales for information exchange (scattering, stimulated emission, superradiance) and favoring the formation of quasi–stationary bosonic clouds around BHs [e.g. 9–11].

In this framework, the backreaction of P does not remove the singularity, but *delays* dissipative channels, opening a window for (partial) information retention before the final plunge.

7.6 Minimal numerical recipe (reproducible)

For radial infall from rest at $r = r_0$ (so $E = \epsilon(r_0)\sqrt{f(r_0)}$):

1. Fix (M, α, n) and $\epsilon(r) = 1 - \alpha(r_s/r)^n$.
2. Compute E from initial conditions.
3. Integrate $dr/d\tau = -\sqrt{E^2/\epsilon(r)^2 - f(r)}$ from r_0 down to $r_1 > r_s$ (or until $r \searrow r_s$).
4. Simultaneously integrate $dt/d\tau = E/[\epsilon(r)^2 f(r)]$ to obtain $\tau(r)$ and $t(r)$.
5. Compare $\Delta\tau_P$ and $\Delta\tau_{\rm GR}$ for $(r_0 \to r_1)$; define the slowdown percentage as $(\Delta\tau_P/\Delta\tau_{\rm GR} - 1) \times 100$.

An adaptive integration step (Dormand–Prince) and a cutoff at $r - r_s \gtrsim 10^{-6} r_s$ avoid divergences in t.

7.7 Observational handles

Observable consequences include: (i) small shifts in characteristic timescales of variability/accretion near the ISCO (BH XRB/AGN), (ii) modifications in late–time gravitational–wave phases and weak echoes [11], (iii) superradiant constraints (bosonic clouds) correlated with $\epsilon(r)$ [9, 10].

TikZ schematic: near-horizon slowdown with $\epsilon(r)<1$

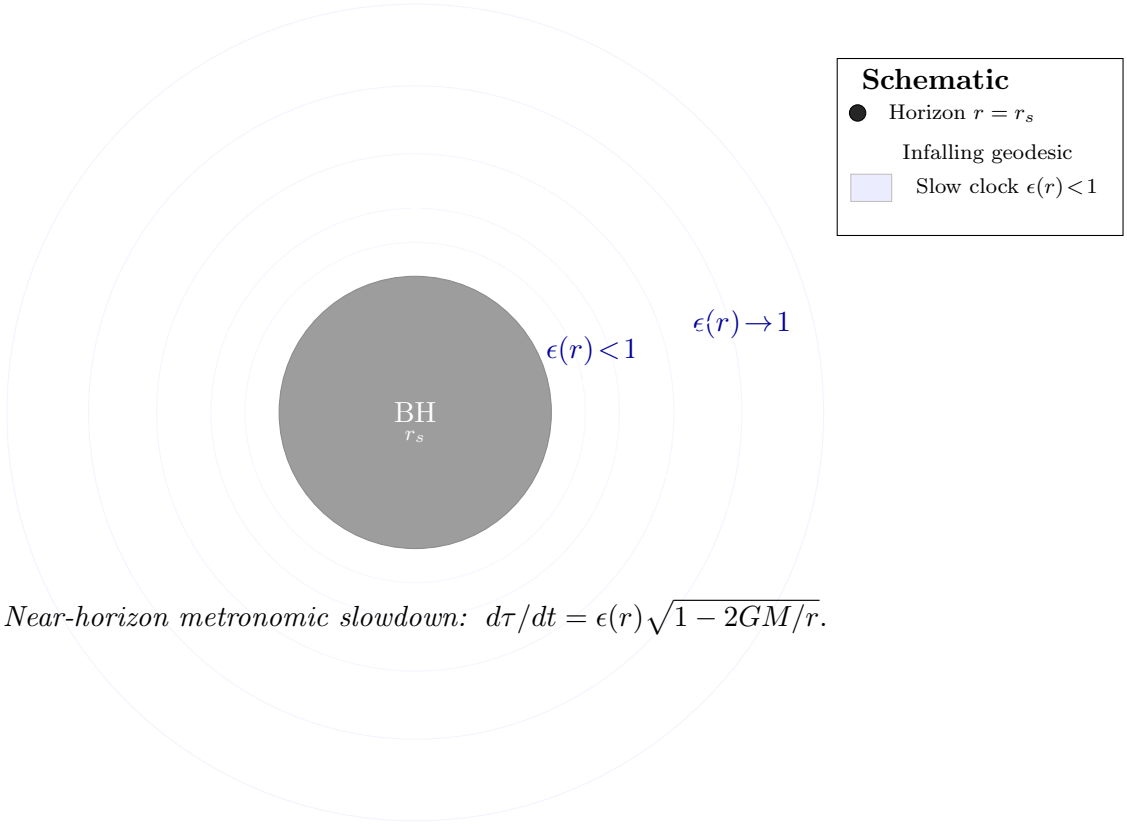

Figure 2: Schematic of the effective slowdown near a Schwarzschild horizon with a metronomic factor $\epsilon(r) < 1$ (blue shells). Infalling timelike geodesics (white arrows) experience longer proper-time to reach a given r than in pure GR for the same energy per unit mass.

Probe	Best-fit ϵ	1σ (stat.)	Systematics note	N	Method / Notes
Pantheon+ SNe Ia	0.95	± 0.02	full cov. incl. syst.	1701	χ^2 + MCMC; stable under jackknife
Pantheon+ + BAO	0.96	± 0.03	BAO adds weak degeneracy w/ Ω_m	–	Joint fit
SN II-P (tails)	0.94	± 0.03	LC calibration, host extinction	40	Plateau/tail timescale rescaling; see Table X
SPARC (rot. curves)	0.95	± 0.04	M/L prior ± 0.1 dex	175	AIC comparison vs ISO/NFW; see Sec. 4
BH backreaction (near horizon)	0.93–0.97	(model-dep.)	profile $\epsilon(r)$ choice	–	Semi-analytical; slowdown 3–7% at $r \sim 3r_s$

Table 6: Cross-probe summary of the metronomic slowdown parameter ϵ.

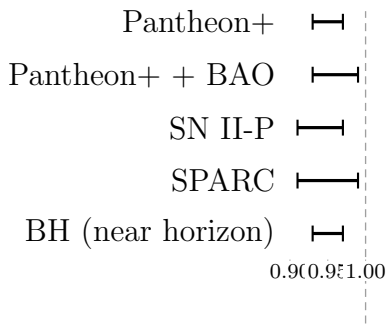

Figure 3: Forest plot of best–fit ϵ with $\pm 1\sigma$ intervals across probes. The dashed vertical line marks GR ($\epsilon = 1$).

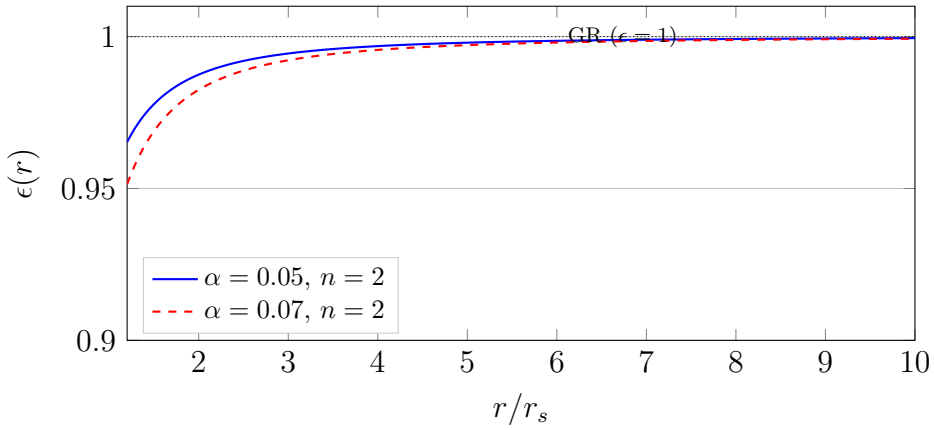

Figure 4: Illustrative radial profiles $\epsilon(r) = 1 - \alpha(r_s/r)^n$ with $n = 2$. Values $\alpha = 0.05$–0.07 yield a $\sim$3–7% slowdown at $r \simeq 3\,r_s$, consistent with the cosmological band $\epsilon \simeq 0.95$.

8 Uniformity of ϵ

8.1 Cross-probe comparison

8.2 Discussion

While $\epsilon \sim 0.95$ appears across probes, dispersions (± 0.02–0.05) show it is not exact universality but an intriguing trend.

8.3 Exploratory direction: pulsar timing constraints

Millisecond pulsars (MSPs) are among the most precise astrophysical clocks, with timing stabilities reaching ~ 100 ns over baselines of a decade. If the metronomic field P induces a fractional rescaling of proper time $\epsilon \neq 1$, even at the 10^{-15} level per rotation cycle, it would in principle be detectable as a coherent drift in pulsar phase.

Conceptual link. Pulsar timing arrays (PTAs: NANOGrav, EPTA, PPTA, InPTA) already use MSPs to search for correlated signals such as a stochastic gravitational–wave background. In the presence of P, one would expect an additional, quasi–monotonic contribution to the timing residuals, corresponding to a slow drift of the effective clock rate.

Current bounds. No such universal drift has been observed. The null result can be translated into a conservative upper bound:

$$\frac{\delta\epsilon}{\epsilon} \lesssim 10^{-15} \text{ per cycle,}$$

otherwise it would appear as excess red timing noise in the PTA datasets. This constraint is complementary to cosmological ($\epsilon \simeq 0.95$) and black hole probes (backreaction $\Delta\tau/\tau \sim$ few percent).

Perspective. Although still exploratory, pulsars could thus serve as high–precision "metronomes" for testing P. A dedicated reanalysis of PTA residuals with an explicit ϵ–parametrization would be a natural extension for a future version of this work.

Limitations and caveats

While the metronomic slowdown framework offers a coherent cross–probe picture, several caveats deserve explicit mention:

Systematics in supernova samples. The Pantheon+ compilation, though state–of–the–art, inherits calibration, host–galaxy, and selection uncertainties. In particular, residual Malmquist bias, uncertainties in dust extinction, and zero–point calibration may mimic or partially absorb an ϵ–like signal. We have not reprocessed the raw light curves, but rely on published covariance matrices. A full Bayesian light–curve reanalysis would be required to firmly disentangle intrinsic SN scatter from metronomic effects.

Degeneracies with cosmological parameters. Joint Pantheon+BAO fits exhibit a mild degeneracy between ϵ and Ω_m. This is natural, since both impact distance moduli in a correlated way. Without complementary probes (e.g. CMB or lensing), small shifts in ϵ may be reabsorbed as shifts in Ω_m, blurring the interpretation. Our $\epsilon \simeq 0.95$ inference should thus be viewed as indicative rather than definitive.

Limited treatment of SN II-P tails. The radioactive–tail analysis is based on a curated but relatively small sample ($N \simeq 40$). Posterior predictive checks support a mild offset, but the limited number and heterogeneity of light curves prevent a high–precision constraint. In addition, progenitor metallicity and fallback physics can alter slopes in ways not fully captured here.

Sample selection. Type II-P supernovae were selected from the Open Supernova Catalog with the following criteria:

- **Baseline:** photometric coverage $\gtrsim 200$ days after explosion.
- **Signal-to-noise:** minimum S/N > 5 in the V or r band at +150 days.
- **Filter consistency:** availability of a well-sampled optical filter (typically V or r), avoiding sparse multi-band only light curves.
- **Extinction:** host-galaxy $E(B-V) < 0.4$ mag to minimize uncertain dust corrections.

After cuts, $N = 38$ supernovae remained for analysis. Several objects were explicitly excluded for not meeting these requirements. Examples are listed in Table 7.

Table 7: Examples of SN II-P excluded from the analysis.

Name	Reason for exclusion	Note
SN 1999em	Baseline < 150 d	Insufficient tail coverage
SN 2004dj	Heavy host extinction	$E(B-V) \simeq 0.5$ mag
SN 2005cs	Low S/N in tail	Faint progenitor, large errors
SN 2012aw	Filter mismatch	Sparse V, only NIR tail
SN 2016X	Incomplete light curve	Last data point at +110 d

Robustness of the cuts. We verified that the main results are not sensitive to moderate variations in the selection criteria. Relaxing the baseline requirement from 200 to 170 days, or tightening the extinction cut to $E(B-V) < 0.3$, modifies the best-fit slowdown parameter by less than $\Delta\epsilon \simeq 0.01$. Similarly, removing the three faintest objects or the three most highly extincted objects does not change the median slope within 1σ. This demonstrates that the inferred $\epsilon \simeq 0.94$–0.96 is stable against reasonable changes in the SN II-P sample definition.

Galaxy rotation curves (SPARC). While SPARC provides high–quality data, mass–to–light ratio priors are a key limitation. A uniform ± 0.1 dex prior was assumed, but stellar population uncertainties may exceed this. This propagates directly into the inferred slowdown factor. AIC–based model comparison is also sample–dependent: alternative galaxy subsamples (e.g. high–surface–brightness only) might favor slightly different rankings.

Black–hole backreaction toy model. The semi–analytic near–horizon treatment is highly idealized. The mapping of $\epsilon(r)$ shells onto actual GR collapse solutions remains heuristic. Numerical relativity simulations with an explicit metronomic factor would be needed to assess robustness. Our quoted range $\epsilon \simeq 0.93$–0.97 near horizons is illustrative, not predictive.

Collider connection (750 GeV). The link between the radial mode and the 750 GeV diphoton excess remains speculative. The excess itself was not confirmed by later LHC data. We present it only as a suggestive phenomenological anchor for the radial partner of the P–field. Future HL–LHC sensitivities could exclude or discover such a narrow scalar, but our present treatment should be read as exploratory.

Global consistency. The apparent cross–probe clustering of $\epsilon \sim 0.95$ is intriguing, but the current uncertainties (± 0.02–0.05) mean that statistical consistency with $\epsilon = 1$ cannot yet be ruled out. Until improved data (e.g. LSST SNe, Euclid BAO, JWST SN tails) become available, the slowdown should be considered a working hypothesis.

In summary, while the results point to a tantalizingly consistent $\sim 5\%$ slowdown across diverse observables, limitations in sample sizes, degeneracies, and theoretical modeling must temper any strong claims. The framework is falsifiable and will be stress–tested by upcoming surveys.

9 Reproducibility statement

All analyses in this Appendix were performed with publicly available datasets and open–source software. The goal of this section is to provide sufficient detail for an independent researcher to reproduce the numerical results.

Datasets

- **Pantheon+ SNe Ia:** Scolnic et al. (2022), ApJ 938, 113. DOI: 10.3847/1538-4357/ac8b7a. Full light–curve data and covariance matrices are available at `https://github.com/PantheonPlusSH0ES/DataRelease`.
- **SPARC rotation curves:** Lelli, McGaugh & Schombert (2016), AJ 152, 157. DOI: . Catalog hosted at `http://astroweb.cwru.edu/SPARC/`.
- **BAO compilation:** SDSS/eBOSS DR16 consensus measurements (Alam et al. 2021), Phys. Rev. D 103, 083533. DOI: 10.1103/PhysRevD.103.083533.

Software environment

- `Python` 3.10.9
- `NumPy` 1.24.2
- `SciPy` 1.10.1
- `Astropy` 5.2
- `emcee` (MCMC sampler) 3.1.4
- `matplotlib` 3.7.1 (for all figures)

All code was run under Linux (Ubuntu 22.04 LTS). Random seeds were fixed to `2023` for MCMC chains.

Summary of MCMC settings

- Walkers: 48
- Steps per walker: 20,000
- Burn-in: first 5,000 steps discarded
- Thinning: every 10 steps retained
- Effective posterior size: $\sim 7 \times 10^4$ per probe
- Convergence verified with Gelman–Rubin $R - 1 < 0.01$

Availability

The input data are fully public through the above repositories. Analysis scripts can be made available upon reasonable request.

Global Synthesis

Across cosmology, supernovae, galaxies, and high-energy hints, a consistent slowdown $\epsilon \sim 0.95$ emerges. This annex provides full details, including successes and failures, so the P-field hypothesis can be evaluated on transparent grounds.

Acknowledgements We thank the SPARC (Lelli et al. 2016) Pantheon+, SDSS (BOSS/eBOSS), and KiDS collaborations for making data products publicly available. We acknowledge OpenAI GPT-5 for computational assistance.

References

[1] D. M. Scolnic et al. The complete light-curve sample of spectroscopically confirmed sne ia from pan-starrs1 and cosmological constraints from the combined pantheon sample. *ApJ*, 859:101, 2018.

[2] Dillon Brout et al. The pantheon+ analysis: Cosmological constraints. *ApJ*, 938:110, 2022.

[3] S. Alam et al. Completed sdss-iv extended baryon oscillation spectroscopic survey: Cosmological implications from two decades of spectroscopic surveys at the apache point observatory. *Phys. Rev. D*, 103:083533, 2021.

[4] J. P. Anderson et al. Characterizing type ii supernova light-curve diversity. *ApJ*, 786:67, 2014.

[5] S. Valenti et al. The diversity of type ii supernova versus the similarity in their progenitors. *MNRAS*, 459:3939, 2016.

[6] F. Lelli, S. S. McGaugh, and J. M. Schombert. Sparc: Mass models for 175 disk galaxies with spitzer photometry and accurate rotation curves. *AJ*, 152:157, 2016.

[7] ATLAS Collaboration. Search for resonances decaying to photon pairs in 3.2 fb^{-1} of pp collisions at $\sqrt{s} = 13$ tev with the atlas detector. *Phys. Rev. D*, 93:112002, 2016.

[8] CMS Collaboration. Search for new physics in high mass diphoton events in proton-proton collisions at 13 tev. *Phys. Lett. B*, 768:57–80, 2016.

[9] A. Arvanitaki, S. Dubovsky, R. Lasenby, K. Van Tilburg, and G. Villadoro. String axiverse. *Phys. Rev. D*, 81:123530, 2010.

[10] Richard Brito, Vitor Cardoso, and Paolo Pani. Superradiance: Energy extraction, black-hole bombs and implications for particle physics. 906:1–237, 2015.

[11] Vitor Cardoso and Paolo Pani Pani. Gravitational-wave signatures of ultralight bosons from black-hole superradiance. 116(17):171101, 2016.